Stanford Exploration Project, Report 75, November 17, 1997, pages 69–88

Gaussian beam migration

Lewei Mo[1]

keywords: *ray tracing, modeling, velocity, reflectivity, diffraction, depth migration*

ABSTRACT

This paper reports on my use of Gaussian beam wave propagation theory to downward continue all the frequency components of individual surface recorded wavefield traces (point sources) into the subsurface. According to the Huygens secondary point source principle, the surface recorded wavefields can be regarded as a series of point sources. The theory of Gaussian beam wave propagation asserts that asymptotic high frequency wavefield components propagate along rays, of which the wavefronts are parabolas and the amplitude profiles overriding the ray paths are Gaussian functions decaying away from the central ray paths. With my method, Gaussian beam wave propagation is implemented in the space-frequency domain. Poststack and prestack common-shot profile migration are accomplished by applying the corresponding imaging condition to the downward continued Gaussian beam wavefields in the frequency domain. The surface seismograms are migrated separately, and the migration process finishes by summing the contributions of all surface recorded traces to obtain the subsurface reflectivity image. This migration scheme combines the advantages of complete wave equation migration and ray tracing based migration. Tests with synthetic data show that the Gaussian beams evaluated along only seventeen rays from each surface seismogram location can image a fairly complex velocity and reflectivity model.

INTRODUCTION

Migration imaging is based on the concept of dephasing. In poststack exploding reflector modeling, many subsurface point sources explode simultaneously at time $t = 0$, and the generated wavefields propagate upward to the earth surface to be recorded. Migration is the process that transfers the surface recorded wavefields into the time $t = 0$ wavefield, which is regarded as the subsurface reflectivity image, by removing the upward propagation phase accumulated by the modeling. For the purpose of dephasing, there are two categories of methods, downward continuation in depth and reverse propagation in time. The first category includes three subcategories, finite-

[1]**email:** not available

difference (Claerbout, 1976, 1985), Kirchhoff integral (French, 1974, 1975; Schneider, 1978), and f-k phase-shift methods (Gazdag, 1978). The second category includes reverse time migration implemented in the space-time domain (McMechan, 1983) and in the f-k domain (Baysal et al., 1983). The dephasing of the f-k one-pass transformation method (Stolt, 1978) is accomplished by mapping from the temporal frequency into the spatial depth wavenumber. However, the idea of migration dephasing is best explained by examining the phase shift method (Gazdag, 1978).

In wave phenomena, the surface recorded wavefields, boundary conditions, are secondary point sources, according to Huygens' wavefront construction principle. And there are many point sources. If the clock is run forward in time, the boundary point source wavefields continue to expand upward; this is the modeling process. If the clock is run backward in time, the boundary point source wavefields focus downward; this is the migration process. The downward continuation in depth and reverse propagation in time of wavefields are equivalent in that they both result in downward focusing of the boundary source wavefields for propagation phase reduction.

The previous migration scheme that explicitly takes the surface recorded seismograms as sources is the reverse-time migration method (Levin, 1983). Reverse-time migration, taking the surface recorded wavefields as boundary conditions (Baysal et al., 1983; McMechan, 1983), actually treats them as a series of parallel point sources.

In common-shot forward modeling, seismic waves are generated by a surface point source, and propagate away; the history wavefields at the boundary receiver locations are the recorded wavefields. The mathematical methods that are used to do the common-shot forward modeling are ray-tracing-based methods (Cerveny et al., 1977), wave-equation-based methods [finite-difference (Kelly et al., 1976) and finite-element], and hybrid methods, such as the Gaussian beam approach (Cerveny et al., 1982).

Gaussian beam depth migration has been implemented by several researchers, Costa et al. (1989) through Gabor transform, Hill (1990) through f-k transform, and Lazaratos and Harris (1990) through $\tau - p$ transform. This paper describes the use of Gaussian beam wave propagation theory to migrate the surface recorded data as a series of individual point sources.

In Gaussian beam common-shot forward modeling, the propagation phase increases downward away from the source at the surface. In contrast, in Gaussian beam depth migration, the propagation phase decreases downward away from the source; that is, the surface recorded data are backprojected into the subsurface to image the high-wavenumber velocity band – the reflectivity. What is needed as additional input is a low-wavenumber velocity background. And in migration, every image point is a receiver.

The Gaussian beam depth migration combines the advantages of raytracing based Kirchhoff depth migration and wave equation migration. With Gaussian beam migration, as with Kirchhoff migration, the recording geometry need not be regular. And, as with wave equation migration, the wavefield is regular in caustic regions.

Moreover, two-point ray tracing is unnecessary for Gaussian beam migration.

This paper first reviews the theory of Gaussian beam wave propagation. Then it demonstrates poststack Gaussian beam depth migration with synthetic data. Finally, it demonstrates prestack Gaussian beam migration, and outlines the procedures for doing Gaussian beam migration using earthquake seismic data.

GAUSSIAN BEAM SOLUTION OF LOCAL PARAXIAL WAVE EQUATION

Gaussian beam wavefield computation is based on the simulation of the wavefield by a system of Gaussian beams by an asymptotic procedure. Since V. Cerveny and his colleagues are largely responsible for the early development of Gaussian beam seismic wave propagation theory, this quotation from their classic paper (Cerveny et al. 1982) is the best introduction to the subject:

> The wave field generated by a line source in a 2-D laterally inhomogeneous medium is decomposed into contributions, corresponding to individual rays. These contributions are evaluated along the rays by the parabolic wave equation method. The parabolic wave equation method gives solutions of the wave equation concentrated close to rays. From the physical point of view these solutions correspond to the Gaussian beams. Each beam is continued independently through an arbitrary inhomogeneous structure. The complete wave field at a receiver is then obtained as an integral superposition of all Gaussian beams arriving in some neighbourhood of the receiver. The corresponding integral formula is valid even in various singular regions where the ray method fails (the vicinity of caustic, critical point, etc.).

The Gaussian beam approach to the problem of wave propagation is to obtain a local paraxial solution to the exact wave equation. The exact monochromatic wave equation is the Helmholtz equation

$$\nabla^2 u(x,z,\omega) + \frac{\omega^2}{v^2(x,z)} u(x,z,\omega) = 0 \tag{1}$$

where ω is the angular frequency and $v(x,z)$ is the wave velocity at the point (x,z). Gaussian beam wavefield computation uses high frequency asymptotic approximation to transform the Helmholtz equation into a parabolic wave equation in ray-centered coordinates (s,n) (Cerveny et al. , 1982, equation (11)), as follows:

$$\frac{2i}{v}\frac{\partial W}{\partial s} + W_{,\nu\nu} - \frac{1}{v^3}\nu^2 \frac{\partial^2 v(s,n)}{\partial n^2} W = 0. \tag{2}$$

The relation between u and W is expressed by the equation $u = \sqrt{v(s)}W(s,\nu)$. Variables s and n are the ray centered coordinates, and $\nu = \sqrt{\omega}n$. The coordinate

s measures the arclength along the ray from an arbitrary reference point, and n represents a length coordinate in the direction perpendicular to the ray at s. The solutions of this parabolic wave equation are evaluated along rays by dynamic ray tracing. And the solutions are called Gaussian beams.

The details of Gaussian beam computation have been given by previous authors (Cerveny et al., 1982; Cerveny, 1983; Cerveny and Psencik, 1984; Nowack and Aki, 1984). Here I summarize them into five steps. Steps (I) and (II) are ray tracing. Steps (III), (IV) and (V) are the computation of wavefields by the Gaussian beam approach.

(I) Conventional kinematic ray tracing – From each surface point source location, a few rays are traced by the standard raypath equations (Cerveny et al., 1977)

$$\frac{dx}{d\tau} = v \sin \sigma \tag{3}$$

$$\frac{dz}{d\tau} = v \cos \sigma \tag{4}$$

$$\frac{d\sigma}{d\tau} = -\frac{\partial v}{\partial x} \cos \sigma + \frac{\partial v}{\partial z} \sin \sigma \tag{5}$$

Variable $v(x, z)$ is the wave propagation velocity, τ is the traveltime along the ray, x and z are the horizontal and vertical Cartesian coordinates along the ray, and σ is the angle between the tangent of the ray at the location (x, z) and the positive z axis. This system of ODEs can be integrated by a standard numerical method, such as the fourth-order Runge-Kutta method. This form of the ray tracing system of equations is very convenient for computation; the traveltime along the ray is just the product of the integration index step and the integration step size $d\tau$, and the ray centered coordinates (s, n) of the depth image points relative to the ray path can be easily computed. At an interface, Snell's law is applied locally.

(II) Dynamic ray tracing – Simultaneously with step **(I)** we integrate the dynamic ray tracing system of ODEs

$$\frac{dQ(s)}{ds} = v(s)P(s) \tag{6}$$

and

$$\frac{dP(s)}{ds} = -\frac{1}{v^2(s)} \frac{\partial^2 v(s,n)}{\partial n^2} Q(s) \tag{7}$$

The scalar functions $P(s)$ and $Q(s)$ are complex. These functions determine the Gaussian beam parabolic wavefront curvature and the Gaussian function amplitude profile.

This system of ODEs can be transferred to the Cartesian coordinate system for computation, as follows:

$$\frac{dQ}{d\tau} = v^2 P \tag{8}$$

and

$$\frac{dP}{d\tau} = -\frac{1}{v}\frac{\partial^2 v(s,n)}{\partial n^2} Q \tag{9}$$

where

$$\frac{\partial^2 v(s,n)}{\partial n^2} = \frac{\partial^2 v}{\partial x^2}\cos^2\sigma - 2\frac{\partial^2 v}{\partial x \partial z}\cos\sigma\sin\sigma + \frac{\partial^2 v}{\partial z^2}\sin^2\sigma \tag{10}$$

(III) Solution of the parabolic wave equation by the Gaussian beam method – Next we calculate the wavefield $u(s,n,\omega)$ associated with the raypath by evaluating the function

$$u(s,n,\omega) = \left[\frac{v(s)}{Q(s)}\right]^{1/2} exp\left\{signum\left[i\omega\tau(s) + \frac{i\omega}{2}\frac{P(s)}{Q(s)}n^2\right]\right\} \tag{11}$$

This is the Gaussian beam. It is an asymptotic local paraxial solution of the complete monochromatic Helmholtz wave equation concentrated close to the ray path. The variable *signum* determines whether the propagation phase increases or decreases, and it is assigned the value $+1$ or -1 depending on whether it is in migration or modeling and on the sign convention of the Fourier transform. The second term in the exponential determines that the wavefront is a parabola and that the amplitude profile is a Gaussian function, hence the name Gaussian beam. The higher the frequency is, the sharper the parabolic wavefront and the narrower the Gaussian amplitude profile. As the ray path is usually curved, Gaussian beam wavefields are evaluated only at a region along the ray at which the ray-centered coordinate system (s,n) is regular called "the regularity region," that is, a region at certain distances from the ray before the system of normals constructed to the ray path intersect.

Gaussian beam solution (11) is well-behaved if

$$Im(P/Q) > 0 \tag{12}$$

and

$$|Q| \neq 0 \tag{13}$$

for all ray path length s. Cerveny et al. (1982) show that it is possible to choose the initial values of $P(s)$ and $Q(s)$ such that inequalities (12) and (13) are always true. And there is latitude in the choice of the initial values $P_0 = P(s=0)$ and $Q_0 = Q(s=0)$. This choice determines the initial width and wavefront curvature of the Gaussian beams. Hill (1990) conveniently designated the initial values of P_0 and Q_0 to be

$$P_0 = \frac{i}{V_0} \tag{14}$$

and

$$Q_0 = \frac{\omega_r L_0^2}{V_0} \tag{15}$$

Parameter $L_0 = 2\pi V_a/\omega_r$ specifies the initial beam width at some reference angular frequency ω_r. And ω_r is chosen to be at the lower end of the seismic data spectrum. V_a is a global spatial average of the velocities occurring in the background velocity model, and V_0 is the velocity at the source point $s = n = 0$.

(IV) Expansion of the wavefields into Gaussian beams – The point source wavefields can be expanded into a series of solutions concentrated close to the rays, the Gaussian beams, as

$$U(s,n,\omega) = (-i\omega)^{1/2} \int_{\phi_0}^{\phi_N} \Psi(\phi) u(s,n,\omega) d\phi \tag{16}$$

The function $\Psi(\phi)$ is a weighting factor for decomposing a point source wavefield into Gaussian beams, and its value depends on the takeoff angle ϕ of the ray. And the angle ϕ is measured from the vertical direction. I implement it as $\Psi(\phi) = \cos(\phi)$ as in Kirchhoff migration.

(V) Construction of the wavefields in the time domain – If we let the spectrum of the source time function be $F(\omega)$, then by Fourier transform, we can construct the time domain wavefields as

$$U(s,n,t) = \frac{1}{\pi} Re \int_0^\infty F(\omega) U(s,n,\omega) exp(-i\omega t) d\omega \tag{17}$$

POSTSTACK GAUSSIAN BEAM DEPTH MIGRATION

For Gaussian beam depth migration, the conventional kinematic ray tracing process is performed to find some ray paths from each surface source point. These ray paths serve as frames for wave propagation. The frequency components of the surface seismogram are then backprojected into the background velocity model as Gaussian beams. This process is accomplished by dynamic ray tracing along the previously found ray paths to obtain solutions to the local parabolic wave equation. The solutions are called Gaussian beams.

For depth migration of zero-offset stack section, the reflectivity image is that of the wavefield at time $t = 0$ when all the reflectors explode; it is produced by evaluating Equation (17) at time $t = 0$. Gaussian beam depth migration is accomplished by superposition of all Gaussian beams from all surface point sources, seismograms, to obtain the earth reflectivity image. The superposition of Gaussian beams is justified by the linearity of the wave equation and the wave phenomenon.

The elements of Gaussian beam migration

To demonstrate the basic elements of Gaussian beam migration and migration in general, I have generated a synthetic section (Figure 1) that contains only one nonzero trace and only one isolated wavelet. The maximum time of the section is 0.512. And the migration is to be done in a model with a constant velocity $v = 1$. Thus the maximum possible depth the section can image is 0.512. In this case, I perform the migration in a depth model with a maximum depth of 1, and use only the vertical ray path from the source. The depth image is shown in Figure 2. The Gaussian beams along one ray path can image the neighborhood of the ray path. The figure also explains the dephasing of migration imaging. The depth difference between the two images is 0.512, thus the phase difference of 2π. The first image appears when the entire upward modeling propagation phase has been exhausted by the Gaussian beam downward propagation, and the second image appears when another propagation phase of -2π has accumulated. The same phenomenon can easily happen in phase shift and finite difference $\omega - x$ depth migration. The figure also demonstrates that as the Gaussian beam propagates, its parabolic wavefront spreads.

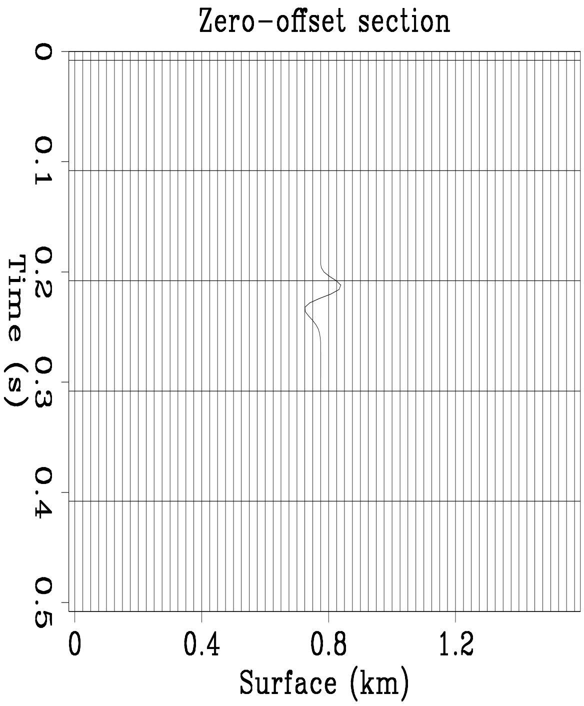

Figure 1: A record section with only one isolated wavelet. mo3-Wavelet.H [ER]

The way to avoid image reappearance is to pad with zeros at the end of the data section, and compute the depth image only to the maximum possible depth. Figure 3 is the depth image generated by migrating the above section with Gaussian beams evaluated along 51 rays from the source, equally spaced from -85 to 85 degrees. For comparison, Figure 4 displays the depth image generated by phase shift migration. In it, Stew Levin's ideas regarding how to avoid wraparound artifacts have been implemented (Levin, 1983; Claerbout, 1985). Here, because the constant velocity $v = 1$, the output of time migration is a depth image. Kinematically, the Gaussian beam migration response correctly matches that of phase shift. However, there is some waveform distortion at high angles. The waveform distortion will be eliminated by careful coordinate interpolation of image points during construction of the Gaussian beams. An advantage of the Gaussian beam migration image over that obtained by the phase shift method is that the image background is much cleaner with Gaussian

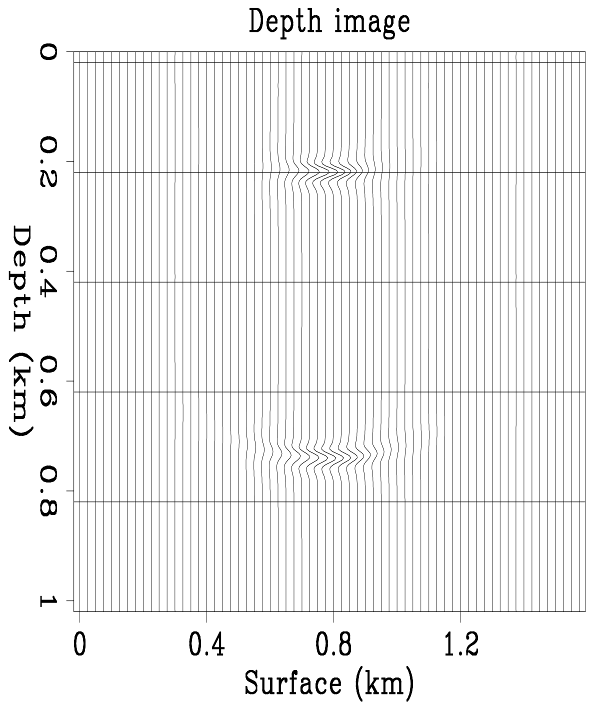

Figure 2: Migration is the process of dephasing. The Gaussian beams along one ray path can image the neighborhood. And as the Gaussian beam propagates, its parabolic wavefront spreads. mo3-DePhase.H [ER]

beam migration.

A smooth v(x,z) background velocity model

Figure 5 shows a smooth background velocity model. Figure 6 is the ray diagram of 17 rays traced down from one surface location by the Runge-Kutta method. The takeoff angles of the 17 rays are equally spaced from -80 to 80 degrees. As the rays are traced in constant increments of traveltime, the spatial distance traversed per step is longer in high velocity zones (long wavelength zones) than in low velocity zones (short wavelength zones), as can be seen from the different spacing between dots along rays. Ray tracing is stopped when the tangent of the ray is close to horizontal. The ray paths correctly follow the background velocity model. Figure 7 is the reflectivity model, with dips ranging from 0 to 45-degree. Figure 8 is the zero-offset section generated by reverse-time migration (Baysal et al., 1983) running in the modeling mode. There is some noise around 0.2 second, generated from the sharp corners of the reflectivity model. Figure 9 is the reflectivity depth image reconstructed by Gaussian beam migration based on ray frames. From each surface source point, 17 rays are traced with takeoff angles equally spaced from -80 to 80 degrees, as in Figure 6. The reconstructed image correctly matches the original reflectivity depth model, and the image background is very clean.

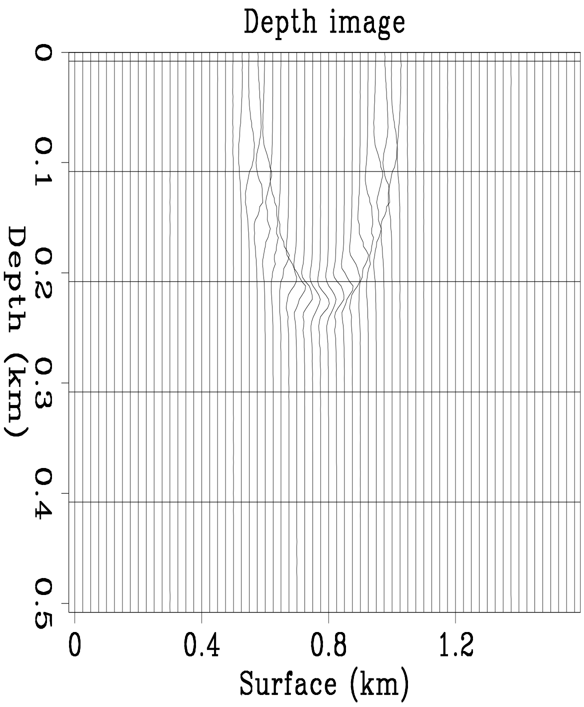

Figure 3: In a constant velocity background model, the migration response of one isolated wavelet is a half circle. This image is produced by Gaussian beam depth migration. mo3-MigGB.H [ER]

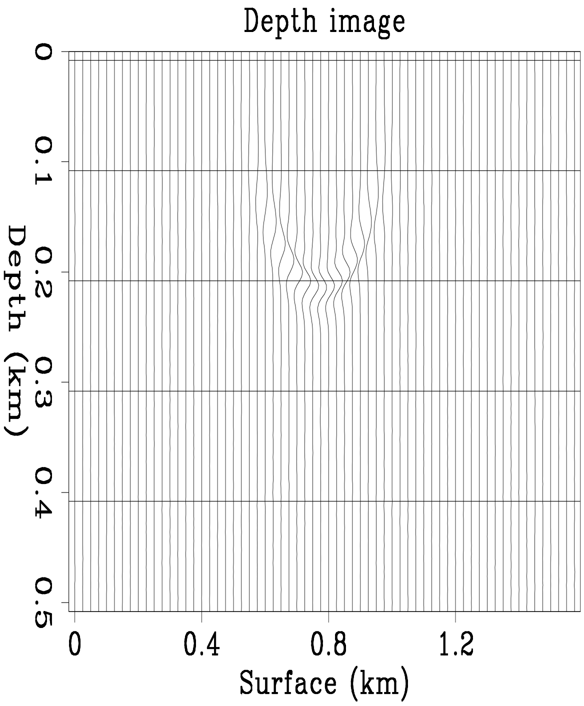

Figure 4: In a constant velocity background model, the migration response of one isolated wavelet is a half circle. This image is produced by phase shift migration. mo3-MigPhase.H [ER]

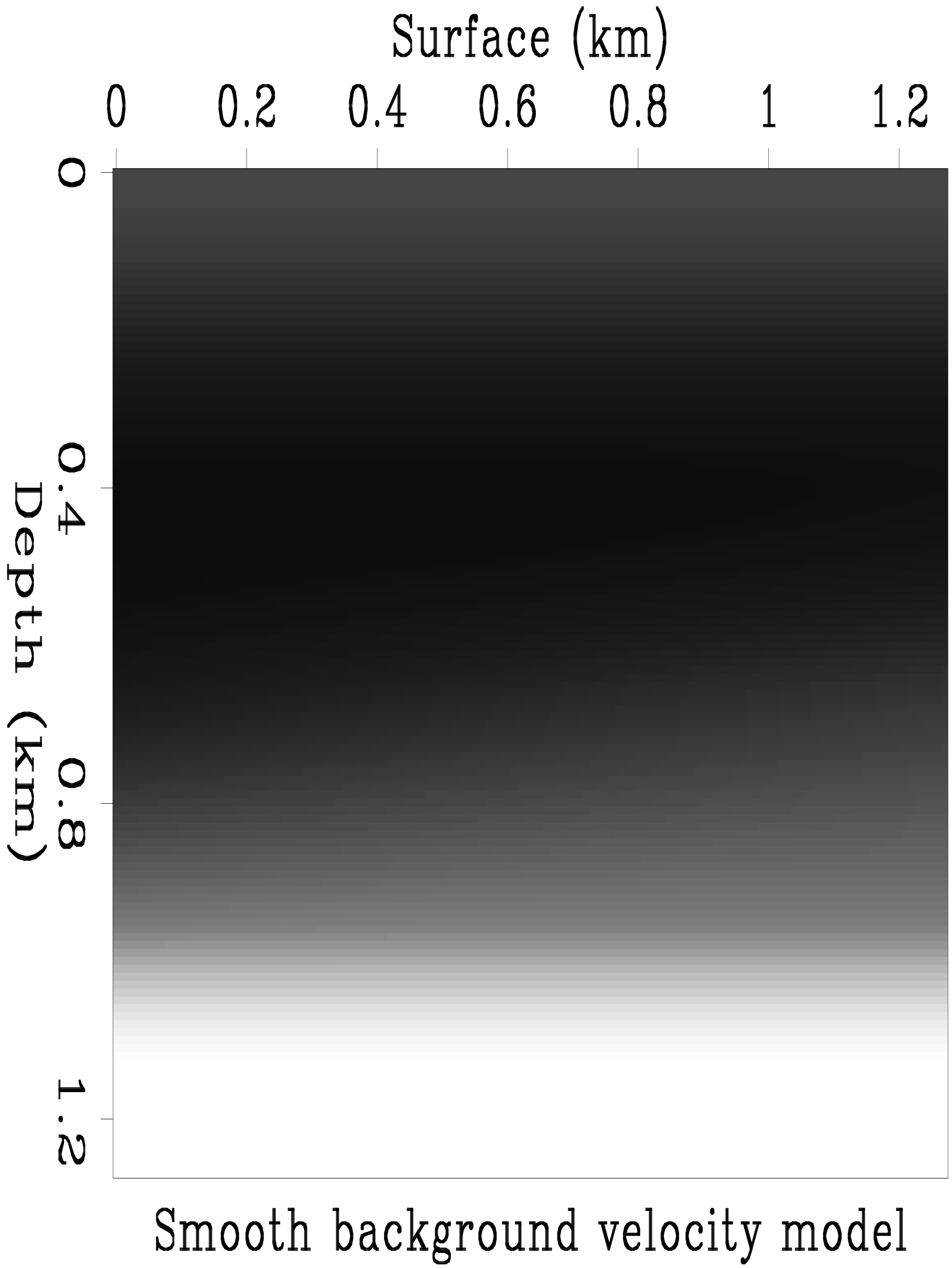

Figure 5: Smooth background velocity model. mo3-Vel.H [ER]

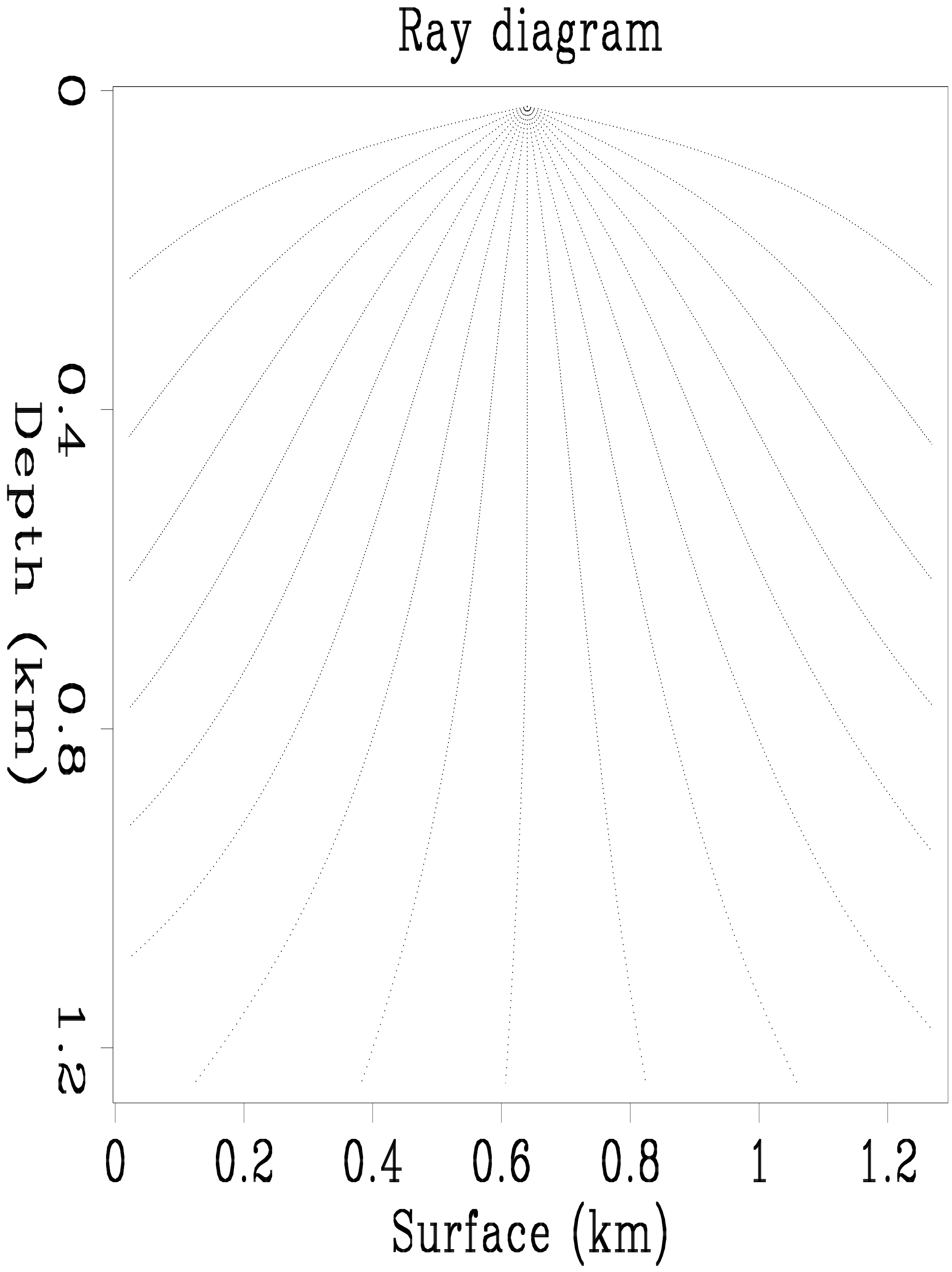

Figure 6: Ray diagrams of 17 rays traced from one surface location through the smooth background velocity model shown in Figure 5. mo3-Ray.H [ER]

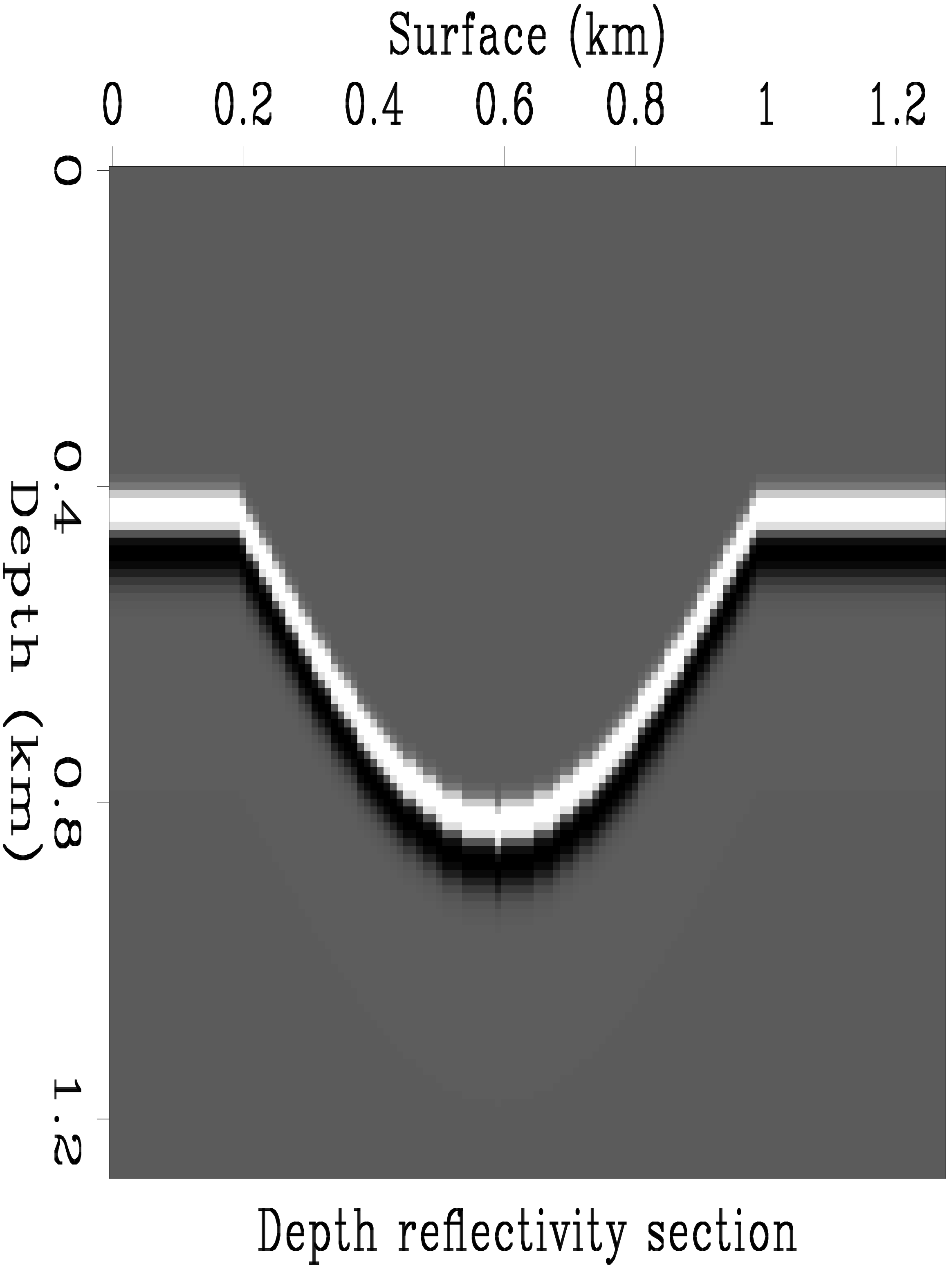

Figure 7: Subsurface depth reflectivity in the smooth background velocity model of Figure 5. mo3-Ref.H [ER]

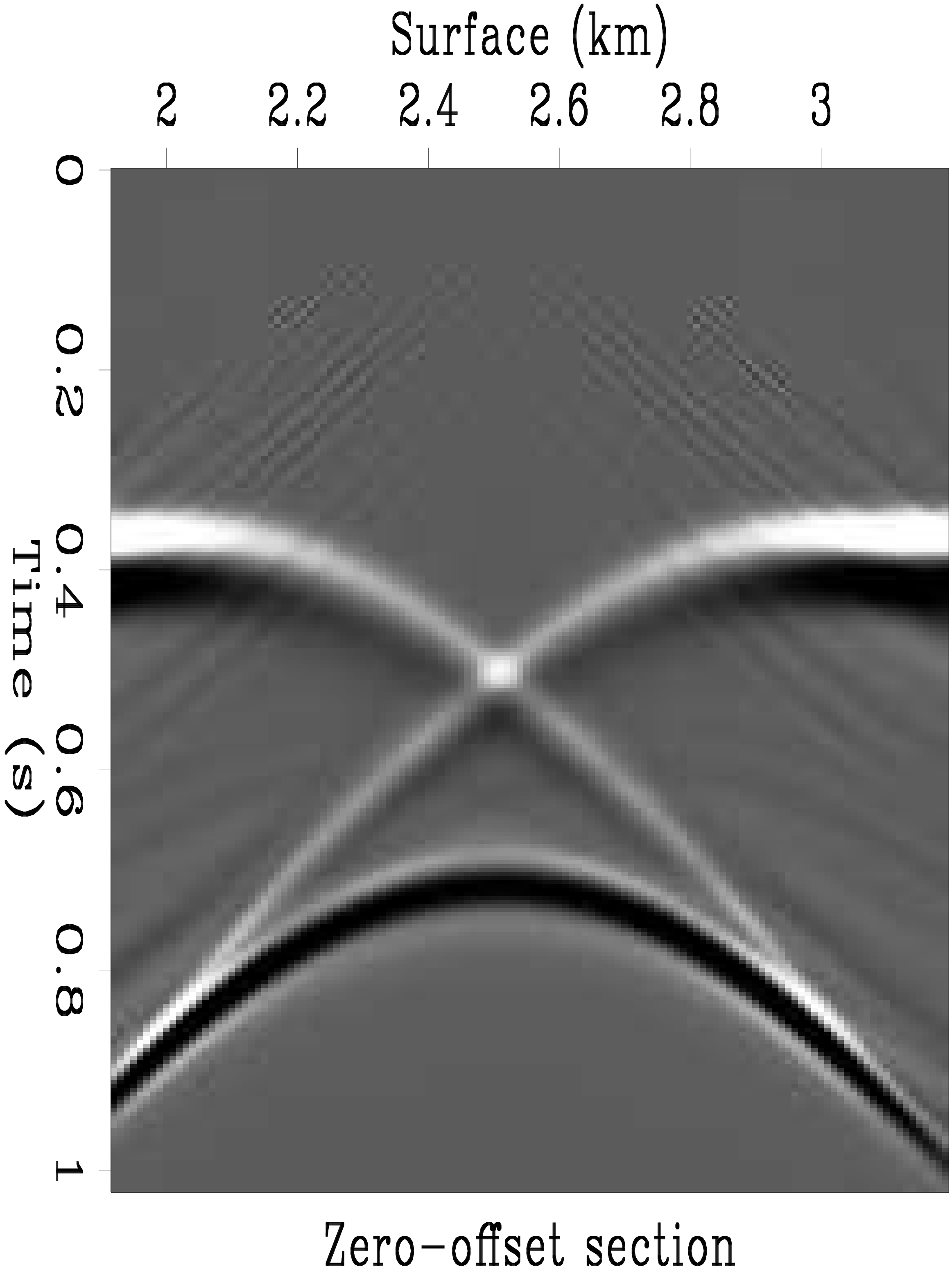

Figure 8: Surface zero-offset section generated by modeling the subsurface depth reflectivity model in the smooth background velocity model with the reverse-time migration method (Baysal et al, 1983). mo3-Section.H [ER]

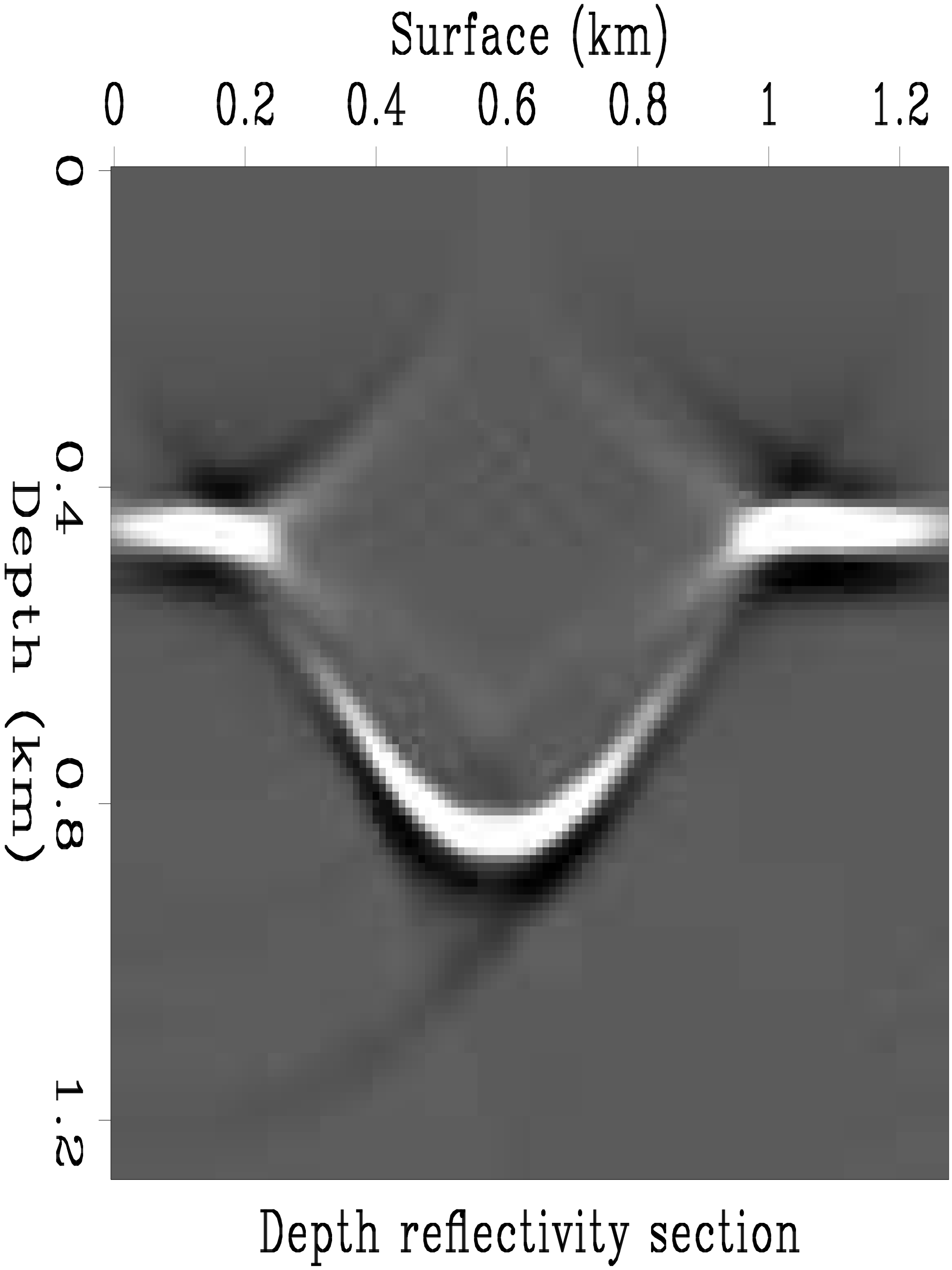

Figure 9: Subsurface depth reflectivity image reconstructed by Gaussian beam depth migration. mo3-ImageGB.H [ER]

PRESTACK GAUSSIAN BEAM DEPTH MIGRATION

The prestack Gaussian beam scheme is implemented as common-shot profile migration, the implementation of which is similar to that of finite difference $\omega - x$ depth migration. All the frequency components of all surface recorded seismograms are downward continued as in the poststack case. The final migrated reflectivity image is obtained after application of the imaging condition to the downward continued wavefields $U(x, z, \omega)$, as in conventional migration (Claerbout, 1976, 1985; Reshef and Kosloff, 1986). When each surface seismogram is taken as a source and migrated separately, the reflectivity image is the wavefield of Equation (17) evaluated at $t = t_d$ at each depth point, where $t = t_d$ is the arrival time of the direct wave from the source to the depth points (x, z). The reflectivity image is formed by superposition of the contributions of all surface seismograms.

Surface and crosswell seismic prestack Gaussian beam depth migration

To demonstrate surface seismic prestack Gaussian beam depth migration, I generate the common-shot gather of Figure 10(a) by ray tracing, modeling a 15-degree dipping reflector in a medium with a constant velocity of 3. The source-receiver near offset is 0.2. Figure 10(b) is the depth image generated by the above stated procedure with the same Gaussian beam computation parameters as in the poststack case. It shows that the method works.

Crosswell seismic prestack Gaussian beam depth migration works the same way. The only difference is in the location of the source.

Earthquake seismic Gaussian beam depth migration

Although the earthquake seismic recording is extremely sparse, there is in fact no lack of information available for migration. When an earthquake occurs, thousands of seismic stations all over the world record the signal. The signal is scattered, diffracted, and reflected throughout the neighborhood of the source. The source position can be located by direct wave traveltime inversion (Aki and Richards, 1980; Stein, 1991). The low wavenumber smooth background velocity model of the earth is assumed to be known. The scattered signal received at the numerous seismic stations is backprojected as Gaussian beams to the neighborhood of the source and the profile migration imaging condition is applied. The migrated image can then been made visible through constructive interference of adjacent wavelets, since we have numerous seismic stations deployed on the earth surface. The result is the high wavenumber velocity band, the reflectivity image of the neighborhood of the source. The records of each earthquake source are then migrated separately to obtain the local images near the sources. Finally, the local images from the many earthquakes are concatenated to form the global reflectivity image.

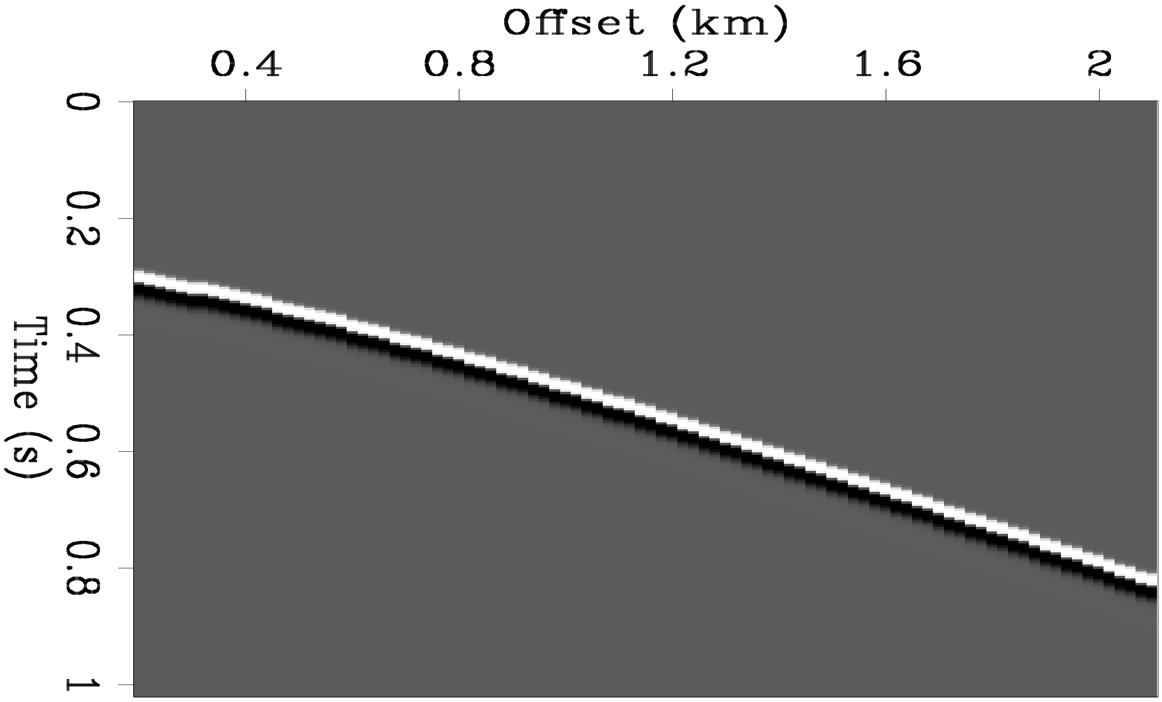

(a) Common−shot gather

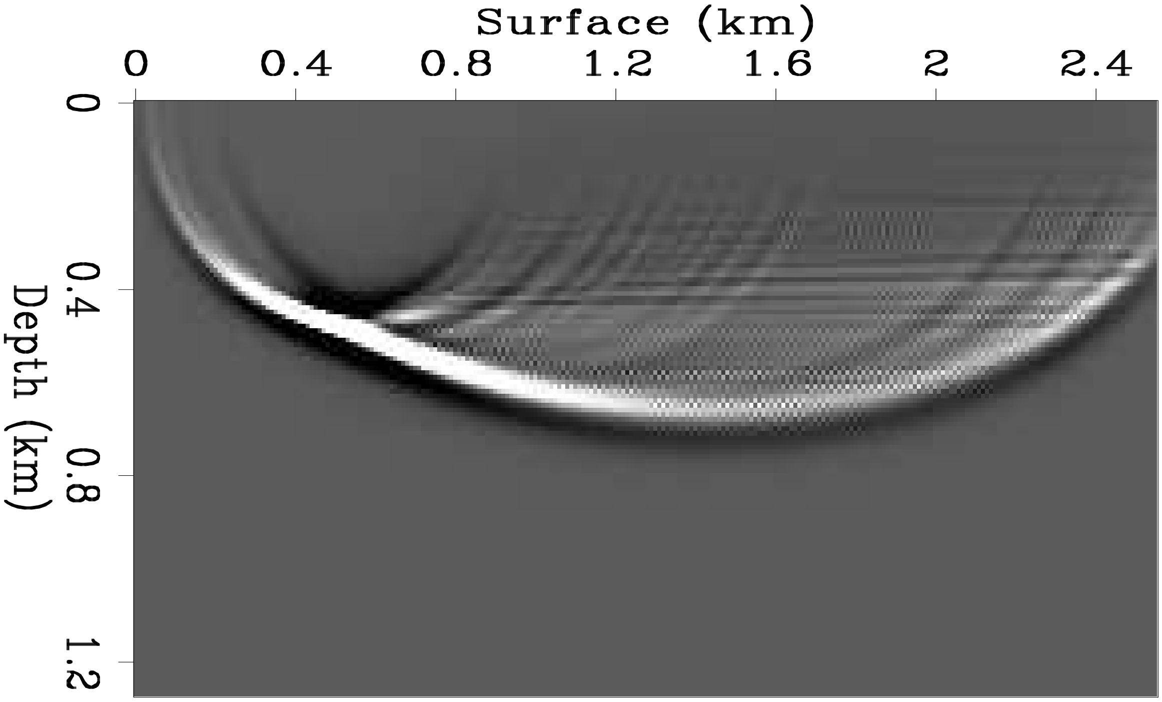

(b) Depth reflectivity section

Figure 10: (a) Common-shot gather generated by ray tracing modeling a 15-degree dipping reflector in a medium with a constant velocity of 3. (b) Subsurface depth reflectivity image reconstructed by prestack Gaussian beam depth migration. The source is at 0.4, and the source-receiver near offset is 0.2. mo3-CSG15Himage [ER]

DISCUSSION

The ray tracing example in this paper shows that ray tracing is stopped when the tangent of the ray is close to horizontal, because all the reflector dips in the reflectivity model are less than 90-degree. This is unnecessary. Ray tracing can be continued as the ray path turns. Computation of Gaussian beams for the turning ray path is equally possible. When this is accomplished, Gaussian beam migration can migrate dips up to 360-degrees. This ability can be of great utility in the migration of earthquake seismic data.

CONCLUSIONS

According to the Huygens secondary point source principle, the surface recorded wavefields can be regarded as a series of point sources. My research has demonstrated the application of Gaussian beam wave propagation theory to downward continue the surface recorded wavefields. Poststack and prestack depth migration are accomplished by applying appropriate imaging conditions to the downward continued wavefields. This research has also demonstrated that the Gaussian beams evaluated along only seventeen rays from each surface seismogram location can image a fairly complex velocity and reflectivity model.

FUTURE RESEARCH

The parameters used in GB computation and the maximum number of rays needed to approximate a point source wavefield should be interrelated. Future research should determine these parameters for efficient computation. In addition, more work is needed to demonstrate the application of Gaussian beams to image complex geological models, such as salt domes. And in general, more work is needed to realize the wide potential of prestack Gaussian beam migration.

ACKNOWLEDGMENTS

My thanks to the sponsors of SEP and its director, Prof. Jon Claerbout, for their generous support. My thanks to the sponsor representatives at the annual Fallen Leaf Lake SEP meeting for their enthusiasms in this research. I am indebted to Jon Claerbout and Biondo Biondi, their talks caught my attention in Gaussian beam migration. I am grateful to Spyroz Lazaratos for stimulating discussions.

REFERENCES

Aki, K., and Richards, P. G., 1980, Quantitative seismology: theory and methods, vol. 1 and 2: W. H. Freeman.

Baysal, E., Kosloff, D. D., and Sherwood, J. W. C., 1983, Reverse time migration: Geophysics, **48**, 1514–1524.

Cerveny, V., Molotkov, I. A., and Psencik, I., 1977, Ray method in seismology: Karlova Univerzita, Prague.

Cerveny, V., Popov, M. M., and Psencik, I., 1982, Computation of wavefields in inhomogeneous media – Gaussian beam approach: Geophys. J. Roy. Soc., **70**, 109–128.

Cerveny, V., 1983, Synthetic body wave seismograms for laterally varying layered structures by the Gaussian beam method: Geophys. J. Roy. Soc., **73**, 389–426.

Cerveny, V., and Psencik, I., 1984, Gaussian beam in laterally varying layered structure: Geophys. J. Roy. Soc., **78**, 65–91.

Claerbout, J. F., 1976, Fundamentals of Geophysical Data Processing: McGraw-Hill.

Claerbout, J. F., 1985, Imaging the Earth's Interior: Blackwell Scientific.

Costa, C. A., Raz, S., and Kosloff, D., 1989, Gaussian beam migration: 59th Ann. Internat. Mtg., Soc. Explor. Geophys., Expanded Abstracts, 1169–1171.

French, W. S., 1974, Two-dimensional and three-dimensional migration model-experiment reflection profiles: Geophysics, **39**, 265–277.

French, W. S., 1975, Computer migration of oblique seismic reflection profiles: Geophysics, **40**, 961–980.

Gazdag, J., 1978, Wave equation migration with the phase-shift method, Geophysics, **43**, 1342–1351.

Hill, N. R., 1990, Gaussian beam migration: Geophysics, **55**, 1416–1428.

Hill, N. R., Watson, T. H., Hassler, M. H., and Sisemore, L. K., 1991, Salt-flank imaging using Gaussian beam migration: 61st Ann. Internat. Mtg., Soc. Explor. Geophys., Expanded Abstracts, 1178–1180.

Kelly, K. R., Ward, R. W., and Treitel, S., 1976, Synthetic seismograms: A finite-difference approach: Geophysics, **41**, 2–27.

Lazaratos, S. K., and Harris, J. M., 1990, Radon transform/Gaussian beam migration: 60th Ann. Internat. Mtg., Soc. Explor. Geophys., Expanded Abstracts, 1314–1317.

Levin, S., 1983, Avoiding artifacts in phase shift migration: SEP–**37**, 27–36.

Levin, S., 1983, Principle of reverse time migration: SEP–**37**, 37–42.

McMechan, G. A., 1983, Migration by extrapolation of time-dependent boundary values: Geophys. Prosp., **31**, 413–420.

Nowack, R., and Aki, K., 1984, The two-dimensional Gaussian beam synthetic method: Testing and application: Journal of Geophysics Research, **89**, 7797–7819.

Reshef, M., and Kosloff, D., 1986, Migration of common shot gathers: Geophysics, **51**, 324–331.

Stein, S., 1991, Introduction to seismology, earthquakes, and earth structures: Department of Geological Sciences, Northwestern University.

Stolt, R. H., 1978, Migration by Fourier transform: Geophysics, **43**, 23–48.